Temperature dependence of the pure rotational band of HD: Interference, widths, and shifts

Z. Lu* and G. C. Tabisz
Department of Physics, The University of Manitoba, Winnipeg, Manitoba, Canada R3T 2N2

L. Ulivi
Istituto di Elettronica Quantistica, Consiglio Nazionale delle Ricerche, Via Panciatichi 56/30, 50127 Firenze, Italy
(Received 23 June 1992)

The far-infrared pure rotational absorption spectra of gaseous HD and HD-X ($X=H_2$, He, Ne, Ar, Kr, and N_2) were measured at 195 and 296 K. Values of the allowed dipole-moment matrix elements, the absolute frequencies, the spectral-line-shape parameters (broadening and frequency-shift coefficients), and the interference parameters, for the first four rotational lines, were deduced from the spectra. Theoretical calculations of the interference parameter a and the linewidths were performed, based, respectively, on the theory developed by Herman, Tipping, and Poll [Phys. Rev. A **20**, 2006 (1979)] and a semiclassical theory developed by Robert and Bonamy [D. Robert and J. Bonamy, J. Phys. **40**, 923 (1979)]. The induced dipole moments for HD-Ne and HD-N_2 were estimated. The analysis includes the present experimental results, together with previous determinations at 77 and 296 K [L. Ulivi, Z. Lu, and G. C. Tabisz, Phys. Rev. A **40**, 642 (1989); P. Drakopoulos and G. C. Tabisz, *ibid.* **36**, 5556 (1987)]. The behavior of the temperature dependence of the collisional interference in the pure rotational band for HD and its mixtures is confirmed to be more complicated than predictions of the intracollisional theory.

PACS number(s): 33.70.Jg, 34.90.+q, 35.20.My

I. INTRODUCTION

Molecular HD is an exceptionally interesting case for studying the interference between allowed-dipole and collision-induced spectra. In recent years, considerable effort has been put forth to study the pressure-broadened infrared-absorption spectrum of the pure rotational band of HD [1]–[13]. The intracollisional interference theory developed by Herman, Tipping, and Poll and co-workers [13–16] seems able to predict an accurate interference strength for the pure rotational line of solid HD, a relatively simple system in which the molecules are fixed in the lattices. The theory does not do so well, however, for the systems of gaseous HD, in which the molecule has more freedom of motion and the molecular interaction is much more complicated than that of solid HD. Therefore, the interference mechanism for gaseous HD is not as clear. This is our second paper [10] focusing attention on the investigation of the pure rotational spectral lines of gaseous HD at different temperatures. The pure rotational absorption spectra of pure HD, HD-(inert gas), HD-H_2, and HD-N_2 at 195 K, and HD-H_2, HD-Kr, and HD-N_2 at 296 K were experimentally investigated with an improved experimental system and data analysis procedure, in the density range of 0–70 amagat. The new experimental data, together with previous results, give a picture of the intermolecular interactions in HD, or between HD and other molecules at 77, 195, and 296 K. Theoretical calculations for interference parameters and linewidths were also performed for comparison with the experimental results. The organization of this paper is as follows. In Sec. II, the relevant theory is given. The improved experiment and data analysis are presented, respectively, in Secs. III and IV. They are followed by theoretical analysis of allowed dipole-moment matrix elements, the interference parameters, and the line-shape parameters according to the existing theories. The paper ends with discussion and conclusions in Sec. VIII.

II. THEORY

The theory of intracollisional interference applied in this study is the semiclassical theory developed by Herman, Tipping, and Poll and co-workers [14–16], and the refinement made by Tabisz and Nelson [3] and Ma, Tipping, and Poll [9]. The total dipole-moment operator of the system, in which the absorbing molecule is immersed in a bath of N perturber molecules, is given by

$$\boldsymbol{\mu}(t)=\boldsymbol{\mu}^A(t)+\sum_j \boldsymbol{\mu}_j^I(t)\ , \tag{1}$$

where $\boldsymbol{\mu}^A$ is the allowed dipole-moment operator of the absorber, and $\boldsymbol{\mu}_j^I$ is the induced dipole-moment operator in a binary collision between absorber and perturber. The induced dipole-moment matrix elements can be expressed in terms of a complete set of eigenfunctions of the total angular momentum [17,18], i.e.,

$$\mu_\nu(\mathbf{r}_1,\mathbf{r}_2,\mathbf{R})=\frac{(4\pi)^{3/2}}{\sqrt{3}}\sum_{\lambda_1,\lambda_2,L,\Lambda} A_\Lambda(\lambda_1\lambda_2 L;r_1,r_2,R) \times\Psi_{1\nu}^{(\lambda_1\lambda_2 L;\Lambda)}(\boldsymbol{\omega}_1,\boldsymbol{\omega}_2,\boldsymbol{\Omega}) \tag{2}$$

or

$$\mu_\nu(\mathbf{r}_1,\mathbf{r}_2,\mathbf{R})=\frac{(4\pi)^{3/2}}{\sqrt{3}}\sum_{\lambda_1,\lambda_2,L,\Lambda}A_\Lambda(\lambda_1\lambda_2L;r_1,r_2,R)\sum_{\mu_1,\mu}C(\Lambda L1;\mu,\nu-\mu)C(\lambda_1\lambda_2\Lambda;\mu_1,\mu-\mu_1)\times Y_{\lambda_1,\mu_1}(\omega_1)Y_{\lambda_2,\mu-\mu_1}(\omega_2)Y_{L,\nu-\mu}(\Omega)\ . \tag{3}$$

Here $\nu=0,\pm1$ is the index of the spherical component related to the Cartesian components according to $\mu_0=\mu_Z$, and $\mu_{\pm1}=\mp(\mu_x\pm i\mu_y)/\sqrt{2}$, the C's are the Clebsch-Gordan coefficients [19] and the Y's are spherical harmonics. R, r_1, and r_2 denote, respectively, the intermolecular distance from absorber to perturber molecule and the internuclear distances within molecules 1 and 2. The real expansion coefficients $A_\Lambda(\lambda_1\lambda_2L;r_1,r_2,R)$, with the same dimension as μ_ν, are thus the components of the pair dipole moment and provide an invariant classification of the induction effects in terms of the parameters λ_1, λ_2, L, and Λ [20]. The dipole-moment correlation function is defined as the ensemble average of the product of the time-correlated dipole moments,

$$C(t)=\langle\boldsymbol{\mu}(0)\cdot\boldsymbol{\mu}(t)\rangle_{\text{ens}}\ . \tag{4}$$

With the substitution of Eq. (1) in Eq. (4), the correlation function responsible for the sharp feature, as shown in Fig. 1, can be written in the form

$$C(t)=C^{AA}(t)+C^{AI}(t)+C^{IA}(t)+C_2^{II}(t)\ , \tag{5}$$

with

$$C^{AA}(t)=\langle\boldsymbol{\mu}^A(0)\cdot\boldsymbol{\mu}^A(t)\rangle_{\text{ens}}\ , \tag{6}$$

$$C^{AI}(t)=N\langle\boldsymbol{\mu}^A(0)\cdot\boldsymbol{\mu}^I(t)\rangle_{\text{ens}}\ , \tag{7}$$

$$C^{IA}(t)=N\langle\boldsymbol{\mu}^I(0)\cdot\boldsymbol{\mu}^A(t)\rangle_{\text{ens}}\ , \tag{8}$$

$$C_2^{II}(t)=N^2\langle\boldsymbol{\mu}_j^I(0)\cdot\boldsymbol{\mu}_k^I(t)\rangle_{\text{ens}}\ , \tag{9}$$

where j and k refer to different perturbers. In the spectrum, the absorption coefficient per unit wave number at frequency ω is given by

$$\frac{\alpha(\omega)}{\omega}=\rho_A N_0\left[\frac{4\pi^2}{3\hbar c}\right][1-\exp(-\hbar\omega/kT)]\phi(\omega)\ . \tag{10}$$

Here ρ_A is the density of the absorber, N_0 is Loschmidt's number, and $\phi(\omega)$ is the spectral line-shape function or spectral density function defined by a Fourier transformation of the correlation function Eq. (4) [7]. Therefore, for a system with $\rho_A N_0$ absorber and ρN_0 perturber molecules ($\rho_A\ll\rho$), with all of the contributions to sharp feature spectrum taken into account, the total absorption coefficient is obtained in the form

$$\frac{\alpha(\omega)}{\omega}=\rho_\alpha N_0\left[\frac{4\pi^2}{3\hbar c}\right](J+1)P(J)\langle J|\mu^A|J+1\rangle^2\left\{[1+2\rho N_0\Delta' I+\rho^2N_0^2(\Delta'^2-\Delta''^2)I^2]\frac{\gamma/2\pi}{(\gamma/2)^2+(\omega-\omega_0)^2}+(\rho N_0\Delta'' I+\rho^2N_0^2\Delta'\Delta''I^2)\frac{2(\omega-\omega_0)/\pi}{(\gamma/2)^2+(\omega-\omega_0)^2}\right\} \tag{11}$$

with

$$P(J)=\frac{e^{-\beta E_J}-e^{-\beta E_{J+1}}}{\sum_K(2K+1)e^{-\beta E_K}}\ . \tag{12}$$

The phase factors Δ' and Δ'' depend on the interacting species and temperature. Due to the *rotational-level mixing*, there is an additional contribution to the integrated absorption coefficient for $R(0)$, and given by [9]

$$\Delta\left[\int\frac{\alpha(\omega)}{\omega}d\omega\right]=\rho_A N_0\left[\frac{4\pi^2}{3\hbar c}\right](J+1)P(J)\langle J|\mu^A|J+1\rangle\frac{\rho N_0}{2\sqrt{2}B_0}\left[\frac{\delta_{J,0}}{2J+1}\right]\times\int_0^\infty\int_0^{2\pi}\int_0^\pi A_2(201;R)V_A(R,\theta)g(R)R^2\sin\theta\,dR\,d\phi\,d\theta\ . \tag{13}$$

Here B_0 is the rotational constant of HD.

The work of Herman, Tipping, and Poll (HTP) was the pioneering theory of the interference effect and predicts the order of magnitude correctly. A more general approach to the problem has recently been given by Gao, Tabisz, Trippenbach, and Cooper (GTTC) [21] for HD-(inert gas) systems. In their treatment the induced and allowed moments are dealt with in a consistent manner and provision is made for effects due to inelastic collisions. In the HTP theory, on the other hand, only non-m or J-changing collisions are considered. Gao, Cooper, and Tabisz [22] have shown explicitly by calculation for HD-He and HD-Ar that inelastic collisions do make important contributions to the interference effect, especially for low initial J values.

The line profile in the theory of GTTC is in general the

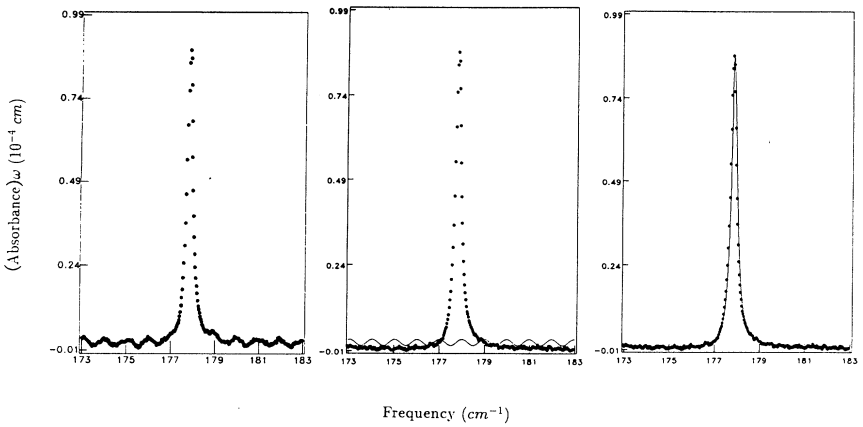

FIG. 1. Spectrum of $R(1)$ for HD-Ne at 195 K. The density of HD is 4.98 amagat and that of Ne is 12.8 amagat. (a) uncorrected data; (b) fitted base curve and corrected base line; (c) corrected spectrum and the fitted curve [Eq. (14)]. The absorbance is $\log_{10}(I_0/I)$, where I_0 and I are the intensities transmitted by the empty and filled sample cells.

sum of Lorentzian and dispersion shapes, characterized through six independent parameters [22]. The HTP profile, on the other hand, requires only four independent parameters (Eq. 11). For elastic, only m-changing collisions, GTTC obtain an expression of the same form as Eq. (11) above; the meaning of the corresponding quantities Δ' and Δ'' is, however, not the same. The correction term given in Eq. (13) represents the effect of rotational level mixing in the limit of no propagation during a collision and is thereby a first approximation to the fuller treatment of GTTC.

In this paper we rely principally on the HTP theory for analysis of the experimental data since the range of densities explored does not permit the specification of the six parameters necessary in the GTTC theory. Moreover, for only a few systems are there sufficiently accurate data available to justify the more extensive calculations required by the GTTC theory. For a full discussion and application of the latter, the reader should consult Refs. [21] and [22].

III. EXPERIMENT

The main experimental aspects are similar to those that have been described elsewhere [10]. A 1-m stainless-steel gas cell is provided with an external container to allow over 92% of the sample cell to be immersed in the coolant bath with a mixture of ethyl alcohol and dry ice at 195 K. The temperature stability over the remaining 3.8 cm from each end of the windows was achieved through thermal conduction by the cell walls and the thick high-pressure flanges. A 6.3-cm-diam. and 3-mm-thick high-density polyethylene disk was compressed between two flanges and served as a window. The cooling-bath container and all connectors to the sample cell were covered with (2–3)-in.-thick foam layer to achieve good thermal isolation. Eight thermocouple detectors were uniformly distributed along the length of the sample cell to monitor the temperature gradient. The high-thermal-conductivity oxygen-free copper sensors of the thermocouples were held in direct mechanical contact with the cell wall by means of teflon clamps. The only temperature gradient was found in the 3.8-cm end regions, and in the worst case, the error in the density determination of the sample gas caused by the incomplete immersion was less than 1%. The vacuum condition was monitored with two CP25-EK Penning gauges and five thermocouple gauges. The vacuum within the sample cell was usually on the order of 10^{-4} Torr when the background spectrum was taken. This vacuum was monitored by a Penning gauge connected directly to the sample cell. An MKS Baratron 220CA absolute-pressure transducer with a PDR-D-1 power-supply digital readout was used to measure the gas pressures below 25 000 Torr. At higher pressures, a Heise gauge was used. The accuracy of MKS baratron was $\pm 0.01\%$ of full scale ± 1 count, while for the Heise gauge it was 0.1% of full scale. HD gas was obtained from MSD Isotropes with a purity of 98%, and the other sample gases all had a purity above 99.99%. A Michelson interferometer system (Nic-7100 Interferometer) with a Nic-660sx computer system was operated at an unapodized theoretical resolution of 0.06 cm^{-1}. The light source was a globar and the detector was a liquid-helium-cooled germanium bolometer. The peak-to-peak voltage of the interferogram V_{pp} was typically 13.7 V at 195 K and 10.7 V at 296 K during the experiment, two times stronger compared to the previous experiments in this laboratory. To reduce the random noise, 400 scans were taken for signal averaging at each density in all cases. The presence of water vapor in the optical path, especially through the variation of its concentration, always introduced noise into the desired spectrum. To solve this problem, more than one background at the same temperature and under the same experimental conditions was recorded. These backgrounds usually contained water lines with different intensities. Some were clean, i.e., contained low-intensity water lines, and some were relatively noisy, i.e., showed strong water absorption. Among the background spectra taken at the same temperature, the cleanest one was taken as a background

file, and the one with the greatest number of water lines was taken as a reference file. The reference file was then adjusted by an appropriate factor determined by when the intensities of strong characteristic water lines (170 and 202 cm^{-1}) in the sample absorbance exactly matched those in the reference absorbance. Finally, the water noise in the sample absorbance spectrum was removed by subtraction. The underlying assumption in this procedure is that the water lines have the same width and frequency in all spectra. This is a good assumption as the water concentration is low and all broadening and frequency shifts occur through interaction of the water molecules with foreign perturbers and not with each other. A virial expansion and the second virial coefficient were used to calculate the amagat density from the pressure data. The virial coefficients at different temperatures were mostly obtained from J. H. Dymond and E. B. Smith [23]. For HD-Kr at 296 K, the virial coefficient was obtained from Ref. [24], where it was estimated following Refs. [25] and [26]. No data were available for HD-Kr at 195 K. For this case, the pressure data at 195 K were converted to the pressure at 296 K based on an ideal-gas model and then the density was determined by using the virial coefficient of HD-Kr at 296 K.

IV. DATA ANALYSIS

The absorbance spectrum within a region of ± 5 cm^{-1} about a sharp rotational line $R(J)$ was fitted by the following equation at every density:

$$\frac{A(\omega)}{\omega}=\frac{D_0}{(\gamma/2)^2+(\omega-\omega_0)^2}+\frac{2(\omega-\omega_0)E_0}{(\gamma/2)^2+(\omega-\omega_0)^2} . \quad (14)$$

This is equivalent to the profile equation introduced by Herman, Tipping, and Poll [16]:

$$\frac{A(\omega)}{\omega}=\frac{D\gamma\pi}{2}\left[(1-q^{-2})\frac{\gamma/2\pi}{(\gamma/2)^2+(\omega-\omega_0)^2}+q^{-1}\frac{2(\omega-\omega_0)/\pi}{(\gamma/2)^2+(\omega-\omega_0)^2}\right] . \quad (15)$$

To improve the base-line correction in the Nicolet system, a straight line $A\omega+BK$ was added to the fitted function. Therefore, there were a total of six adjustable parameters taken in this procedure; base-line correction factors A and BK, the full width at half maximum intensity (FWHM) γ, the shifted line peak frequency ω_0, the intensity parameter D_0, and the asymmetry parameter E_0. A statistical analysis system computer program employing Marquardt algorithms was used in the fitting process. Occasionally there was an oscillatory-type noise, or sine noise, that appeared in the spectra. This was caused by the interference from internal reflections resulting from the parallel surfaces of a window, and the interference fringes present in the sample and background spectra did not cancel [12,27]. However, a sine function was found adequate to represent this type of noise. Thus, for the spectra with such noise, the base line (with the peak region removed) was first fitted by a sine function plus a straight line, and then the noise was subtracted numerically from the spectra before the profile fitting procedure. Figure 1 demonstrates the effectiveness of this approach; (a) shows spectrum with sine noise before correction, (b) is the fitted sine wave and corrected base line, (c) shows the corrected spectrum with the fitted curve given by Eq. (14).

According to the intracollisional theory discussed above, the integrated absorption coefficient may be expressed as follows [14,16]:

$$\int\frac{\alpha(\omega)}{\omega\rho_A N_0}d\omega=\int\frac{\alpha^A(\omega)}{\omega\rho_A N_0}[1+2\rho N_0\Delta' I+\rho^2 N_0^2(\Delta'^2-\Delta''^2)I^2]d\omega$$
$$=C_0+C_1\rho+C_2\rho^2 . \quad (16)$$

The allowed dipole-moment matrix elements and the interference parameter a were deduced from the fitted parameters C_0, C_1, and C_2 [10] by the comparison of Eq. (16) with Eq. (11). The other interference parameter $N_0 I\Delta''$ was obtained by introducing a parameter q such that

$$q^{-1}(\rho)=\frac{\rho N_0\Delta'' I}{1+\rho N_0\Delta' I} , \quad (17)$$

where q^{-1} was calculable from the fitted parameters by comparison of Eq. (14) with Eqs. (15) and (16):

$$q^{-1}(\rho)=\frac{E_0\gamma/D_0}{1+[1+(E_0\gamma/D_0)^2]^{1/2}} . \quad (18)$$

The use of the expression (17) assumes that the HTP rather than the GTTC theory applies. However the determination of q^{-1} through Eq. (18) is independent of the theory used. In the fitting of Eq. (16), the spectral parameters at zero perturber density of the HD-X experiments were first determined. These values were added to the HD-HD data to improve the accuracy of the intercept determination.

All fitting was weighted with the error calculated from the statistical error of parameters in the profile fitting. An estimated error in the density determination was also included. The density-dependent linewidth FWHM and the frequency-shift coefficient were obtained from the profile fitting parameters γ and ω_0 [10,7]:

$$\gamma=B_0\rho+K_0 , \quad (19)$$

$$\omega_0=S_0\rho+\omega_0^0 , \quad (20)$$

where K_0 and ω_0^0 are the linewidth and frequency at zero perturber density, respectively. In the case of HD-HD, ω_0^0 is the absolute frequency of the individual $R(J)$ lines. They were calibrated with the water lines measured with the sample cell under vacuum, and compared with the highly accurate water line frequencies measured by Johns [28].

V. ALLOWED DIPOLE-MOMENT MATRIX ELEMENTS

The allowed dipole-moment matrix elements deduced from the HD-HD and HD-X spectra at different temper-

TABLE I. Magnitude of the matrix elements of the allowed dipole-moment transitions of HD (10^{-4} D) deduced from HD-HD and HD-X systems. The uncertainty (1σ) appears in parentheses.

System	T (K)	$\langle J\|\mu^A\|J+1\rangle$ $J=0$	$J=1$	$J=2$	$J=3$
HD-HD	77[a]	7.19(3)	7.68(4)	8.79(6)	
	195[a]	8.03(12)	8.01(4)	8.12(6)	7.84(23)
	195[b]	8.75(4)	8.09(3)	8.15(2)	8.62(15)
	296[c]	8.83(28)	7.94(2)	7.88(3)	8.43(10)
HD-H_2	77[a]	7.30(15)	7.93(11)	9.17(29)	
	195[b]	8.76(49)	8.32(5)	8.29(5)	8.39(15)
	296[b]		8.18(6)	8.05(6)	8.84(12)
HD-He	77[a]	7.35(12)	7.83(5)	8.79(13)	
	195[a]	12.2(34)	8.78(7)	8.76(7)	11.1(30)
HD-Ne	77[a]	7.95(9)	8.77(13)	7.44(12)	
	195[b]	8.61(10)	8.33(5)	8.25(3)	
HD-Ar	195[a]	7.78(8)	7.93(3)	8.18(5)	8.07(30)
	195[b]	8.73(5)	8.08(5)	7.97(7)	8.19(16)
HD-Kr	195[b]	8.72(4)	8.47(11)	7.96(12)	8.43(11)
	296[b]		8.11(7)	8.09(5)	9.22(13)
HD-N_2	195[b]	8.93(12)	8.29(9)	8.49(8)	7.91(34)
	296[b]		8.31(7)	8.12(5)	8.73(19)

[a]Experiment 1 [10].
[b]Experiment 2. This work.
[c]Experiment 3 [8,24].

atures, including our earlier work [7,10], are collected in Table I. The values in Table I are in general reasonably consistent except for HD-He at 195 K, for which case we failed to remove effectively the underlying water noise, thereby causing the intensity measurements for $R(0)$ and $R(3)$ to be far from accurate. Table I also reflects the fluctuations among the different experiments at different temperatures and among the different experiments at the same temperature. There is not sufficient evidence to suppose a systematic trend with temperature at a given J. Therefore it is justified to perform a weighted average over all the measurements for a given J. It is obvious that the results from HD-HD play an important role in the averaging process because of their good signal-to-noise ratio and the consequent small statistical errors in the fitted parameters. The dipole moments so averaged

TABLE II. Allowed dipole-moment transitions of HD (10^{-4} D). Uncertainty appearing in parentheses for present work is 3σ (this table only).

Reference	$\langle J\|\mu^A\|J+1\rangle$ $J=0$	$J=1$	$J=2$	$J=3$
	Experiment			
Present work[a]	8.10(15)	8.04(12)	8.16(12)	8.55(42)
Present work[b]	7.77(12)	7.95(12)	8.12(9)	8.41(40)
	Calculations			
Wolniewicz[c]	8.36	8.38	8.39	8.41
Ford and Browne[d]	8.31	8.30	8.28	8.26
Thorson, Choi, and Knudson[e]	8.463	8.455	8.440	8.420
Bishop and Cheung[f]	8.65			

[a]Averaged over HD-HD and HD-X spectra.
[b]Averaged over HD-HD spectrum only.
[c]Reference [32].
[d]Reference [29].
[e]Reference [30].
[f]Reference [31].

are presented in Table II, together with the average results from only HD-HD, the experimental results of other workers, and the theoretical calculations. For the average dipole moment, three standard deviations are taken as the uncertainty appearing in parentheses. Thus the average value with its uncertainty is at the 99% confidence level. The experimental values of allowed dipole moments agree quite well with the theoretical calculations in general, and favor the calculation of Wolniewicz in particular. Figure 2 shows the experimental results plotted with the theoretical calculations. Although the calculation of Ford and Browne is close to the experimental values, the J dependence is different. We should point out that the measured J dependence in our experimental result is not predicted by any of the calculations. Within the 99% confidence error bars, the J dependence predicted by Wolniewicz is possible; namely, the magnitude of the allowed-dipole moment increases with increasing of J, while the opposite J dependence seems to be ruled out. If the J dependence can be represented by [35]

$$\mu^A=\mu_0^A+\delta(J+1)^2 , \tag{21}$$

our experimental results yield

$$\mu^A=[8.012+0.019(J+1)^2]\times10^{-4}\ \mathrm{D} , \tag{22}$$

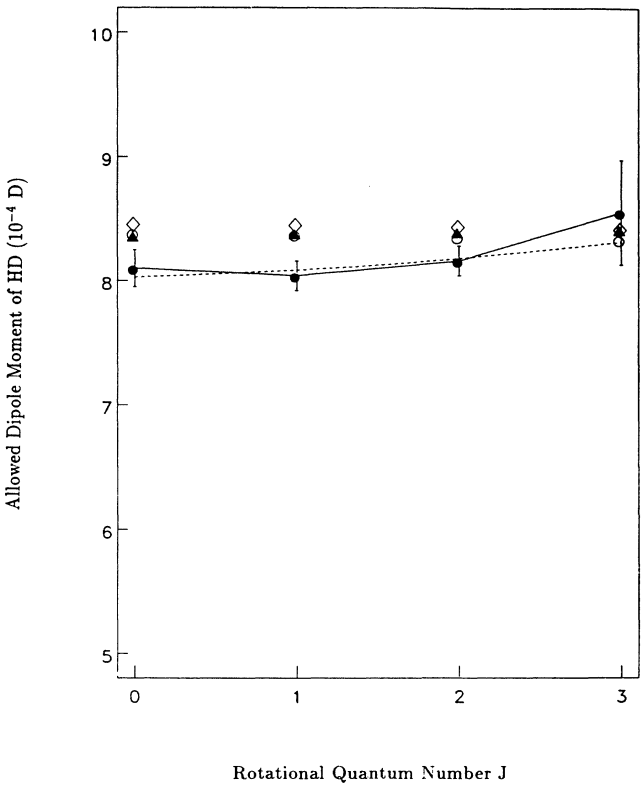

FIG. 2. Comparison of our experimental results with theoretical calculations. The dotted line represents Eq. (22). ●, experimental; ○, Ref. [29]; ◇, Ref. [30]; ▲, Ref. [32].

as illustrated by the dotted line in Fig. 2. Neglecting the J dependence, one obtains an average dipole moment, $(8.11\pm0.14)\times10^{-4}$ D, 3% low with respect to the averaged value of the theoretical calculations. It is interesting to note that although the magnitudes of the dipole moments obtained by Trefler and Gush are far lower than ours, the J dependence is similar [34].

VI. INTERFERENCE PARAMETERS

A. $a=2N_0\Delta' I$

The interference parameter a can be positive (constructive interference) and negative (destructive interference). The experimental interference parameter a, including the results at 77 K, are presented in Table III. The general trends in the experimental a may be summarized as follows:

(i) The parameter a changes sign for all J from 77 to 296 K for HD-HD.

(ii) For HD-atom and for a given temperature, a is positive for all J and all systems at 77 K; at 196 K, usually, a is positive for $R(0)$, $R(2)$, and $R(3)$, but negative for $R(1)$; at 296 K, usually, a is positive for $R(2)$ and $R(3)$ while negative for $R(1)$.

(iii) Consider now a given J, a is mostly positive for $R(0)$ for all temperatures and all systems in general; for $R(1)$, a changes sign frequently for all systems; for $R(2)$ and $R(3)$ there is less frequent sign change in a.

(iv) For a given system, the sign change of a with temperature occurs at low J for small perturber such as He, Ne, and so on, but at high J for large perturbers such as Kr and N_2.

(v) Usually the small perturbers give mostly constructive interference while large perturbers give mostly destructive interference for all J and at all temperatures.

In order to compare our experimental results with theory, we estimated the interference parameters a and Δa, based on the theory developed by Herman, Tipping, and Poll, and co-workers with refinements introduced by Tabisz and Nelson and by Ma, Tipping, and Poll [3,9,14,16]. In the so-called *gentle-encounter limit*, Δ' remains real and essentially equal to unity [16]. At this limit the interference parameter a is given by [35]

$$a=\frac{2N_0\int_0^\infty \mu_{jj'}^I(R)g(\mathbf{R})d\mathbf{R}}{\langle J|\mu^A|J'\rangle} \tag{23}$$

or

$$a=\frac{2N_0\int_0^{2\pi}\int_0^{\pi}\int_0^{\infty}\mu_{jj'}^{pI}(R)g(R)R^2\sin\theta\,d\varphi\,d\theta\,dR}{\langle J|\mu^A|J'\rangle} . \tag{24}$$

In Eq. (23), $\mu_{jj'}^I(R)$ is the induced dipole component with the same symmetry as the allowed-dipole component, i.e., $A_1(100;r_1r_2R)$, and $g(R)$ is the pair-correlation function. In classical statistical mechanics, it is expressed to the zeroth order as [3,36]

$$g(R)=\exp[-\beta V(R)] , \tag{25}$$

where $\beta=(kT)^{-1}$, R is the intermolecular separation, and

$V(R)$ is the intermolecular pair potential, which was obtained from the Taylor expansion of $V_{H_2\text{-}X}(R)$ with respect to the shift of the center of mass [10,18]. Carrying out the integral over φ and θ, one obtains the following expression for a [35]:

$$a=\frac{8\pi N_0}{\langle J|\mu^A|J'\rangle}\int_0^\infty \mu_{jj'}^I \exp[-V_{H_2\text{-}X}(R)\beta] \times\left\{\frac{\sinh[V'_{H_2\text{-}X}(R)\beta r_e/6}{V'_{H_2\text{-}X}\beta r_e/6}\right\}R^2dR \ , \tag{26}$$

$$\mu_{jj'}^I(R)=\langle J|A_1(100;r_1,r_2,R)|J'\rangle \ , \tag{27}$$

where r_1 and r_2 denote the internuclear distances of molecule 1 and 2, and R is the intermolecular distance between the centers of mass. To calculate an additional contribution to the intracollisional interference of $R(0)$ caused by rotational-level mixing, we apply the same potential and pair-correlation function from the calculations of a, and obtain the following expression for Δa [35]:

$$\Delta a=\frac{4\pi N_0}{\langle J|\mu^A|J'\rangle\sqrt{2}B_0\beta} \times\int_0^\infty A_2^{HD\text{-}X}(201;R)\exp[-\beta V_{H_2\text{-}X}(R)] \times\frac{[1-(r_e/6)\beta V'_{H_2\text{-}X}(R)]}{(r_e/6)\beta V'_{H_2\text{-}X}(R)} \times\sinh[(r_e/6)\beta V'_{H_2\text{-}X}(R)]R^2dR \ . \tag{28}$$

Because of the nature of the perturbation theory, the integral in Eq. (28) cannot be taken to small R and it must be cut off so that the first-order wave function remains accurate [3]. This was done following the criteria of Ref. [3]. In the numerical evaluations of a and Δa, $r_e=0.763\,18$ Å or $1.4422a_0$ [10]. Values of $A_\Lambda(\lambda_1\lambda_2L;R)$ used are from the *ab initio* calculations of Borysow, Frommhold, and Meyer [37]. For HD-Kr, only the strength of the induced dipole $A_0^{H_2\text{-}Kr}(001;R)$ in the translational band of H_2-Kr has been semiempirically calculated by Poll and Hunt [38]. Thus, only $A_1^{HD\text{-}Kr}(100;r_1r_2R)$ is calculated from $A_0^{H_2\text{-}Kr}(001;R)$ by a coordinate transformation [14]. The numerical results

TABLE III. Interference parameter a (10^{-3} amagat^{-1}). The uncertainty (1σ) appears in parentheses.

Sample	T (K)	$R(0)$	$R(1)$	$R(2)$	$R(3)$
HD-HD	77[a]	+3.1(4)	+2.2(2)	−3.7(8)	
	195[b]	−2.86(25)	−0.5(2)	+0.20(14)	−12.6(8)
	296[c]	−2.5(19)	−1.1(2)	+1.31(1)	+2.1(6)
HD-H_2	77[a]	+5.4(15)	+2.2(14)	+0.8(29)	
	195[b]	+2.0(13)	−3.6(5)	+0.14(40)	−6.2(41)
	296[b]		−7.1(11)	−7.62(79)	−4.4(18)
HD-He	77[a]	+6.0(16)	+6.2(7)	+4.4(15)	
	195[a]	−11.4(38)	−0.4(9)	+2.34(92)	+3.5(28)
	296[c]		+5.7(9)	+3.9(8)	+10.0(19)
HD-Ne	77[a]	+5.8(15)	+8.5(9)	+7.4(24)	
	195[b]	+4.7(12)	−1.0(4)	+4.34(23)	+12.2(29)
	296[c]		+2.1(4)	+6.9(4)	+5.3(12)
HD-Ar	195[b]	+1.08(97)	−3.93(72)	+9.5(67)	+2.5(31)
	296[c]		+1.8(3)	+6.1(2)	+9.4(11)
HD-Kr	195[b]	+3.8(11)	−18.4(21)	+11.3(25)	+13.8(93)
	296[b]		−19.3(14)	−8.63(69)	−7.1(12)
HD-N_2	195[b]	+15.8(47)	−10.6(21)	+4.2(13)	+12(10)
	296[b]		−22.2(14)	+8.28(82)	−4.5(25)

[a]Experiment 1 [10].
[b]Experiment 2. This work.
[c]Experiment 3 [8,24].

for a and Δa at 77, 195, and 296 K for the various systems (for which the necessary data for such calculations are available) are presented in Table IV. Also given are the calculations of $\Delta a'$ for HD-HD made by Ma, Tipping, and Poll [9], in which a near-resonance rotational-level mixing mechanism was considered for $R(2)$ and $R(3)$.

Comparing the experimental interference parameter a with a_{theory} we find that about 57% agree well on the magnitude only; 63% agree on the sign (HD-Kr not included) only; 34% agree reasonably well on both sign and the magnitude (HD-Kr not included). The better agreement between experiment and theory is found for $R(2)$ and $R(3)$ for HD-atom systems.

B. Induced dipole moment for HD-Ne and HD-N_2

If such agreement is taken as a demonstration of the suitability of the theory, we can then use it to estimate the induced dipole moment for HD-Ne and HD-N_2 from the experimental interference parameter a. It is assumed that the induced dipole moments for HD-Ne and HD-N_2 are dominated by the isotropic overlap component, which is normally true [37], and have the form [38]

$$\mu^I(R) = Ae^{B(R-R_0)}, \tag{29}$$

where R is the intermolecular distance and A, B, and R_0 are parameters to be determined. Then we have the following integral equation:

$$1.236\,57a = A\int_0^\infty \exp[B(R-R_0) - V_{H_2\text{-}X}(R)\beta] \times \left\{\frac{\sinh[V'_{H_2\text{-}X}(R)\beta r_e/6]}{V'_{H_2\text{-}X}\beta r_e/6}\right\} R^2 dR \,. \tag{30}$$

From the experimental results, at different temperatures, three integral equations can be constructed for HD-Ne and two for HD-N_2. The potentials used in the calcula-

TABLE IV. Calculated interference parameters a and Δa (10^{-3} amagat^{-1}). The values of a and Δa are found using Eqs. (26) and (28), respectively. The value used for a_{theory} is $a+\Delta a+\Delta a'$ for HD-HD or $a+\Delta a$ for HD-X; the sign for the case HD-Kr is unknown.

Sample	T (K)	Parameter	$R(0)$	$R(1)$	$R(2)$	$R(3)$
HD-HD	77	a	+1.04	+1.04	+1.04	
		$a+\Delta a$	+1.33	+1.04	+1.04	
		a_{theory}	+1.33	+1.04	−2.36	
	195	a	+1.48	+1.48	+1.48	+1.48
		$a+\Delta a$	+2.12	1.48	1.48	1.48
		a_{theory}	+2.12	+1.48	−1.62	+1.28
	296	a	+1.86	+1.86	+1.86	+1.86
		$a+\Delta a$	+2.79	1.86	1.86	1.86
		a_{theory}	+2.79	+1.86	−1.34	+1.66
HD-H_2	77	a	+0.73	+0.73	+0.73	
		a_{theory}	+1.05	+0.73	+0.73	
	195	a	+1.17	+1.17	+1.17	+1.17
		a_{theory}	+1.85	+1.17	+1.17	1.17
	296	a	+1.52	+1.52	+1.52	+1.52
		a_{theory}	+2.51	+1.52	+1.52	+1.52
HD-He	77	a	+4.46	+4.46	+4.46	
		a_{theory}	+4.49	+4.46	+4.46	
	195	a	+6.18	+6.18	+6.18	+6.18
		a_{theory}	+6.27	+6.18	+6.18	+6.18
	296	a	+7.36	+7.36	+7.36	+7.36
		a_{theory}	+7.49	+7.36	+7.36	+7.36
HD-Ar	195	a	+8.83	+8.83	+8.83	+8.83
		a_{theory}	+9.29	+8.83	+8.83	+8.83
	296	a	+9.49	+9.49	+9.49	+9.49
		a_{theory}	+10.17	+9.49	+9.49	+9.49
HD-Kr	195	a	11.5	11.5	11.5	11.5
		a_{theory}	11.5	11.5	11.5	11.5
	296	a	11.66	11.66	11.66	11.66
		a_{theory}	11.66	11.66	11.66	11.66

TABLE V. Estimated parameters A (10^{-4}D), B (Å^{-1}), and R_0 (Å) of induced dipole moment [Eq. (30)].

System	A	B	R_0
HD-Ne	−6.5	−3.03	2.99
HD-N_2	−12.8	−2.89	3.15
H_2-Ar[a]	10.0	−2.86	3.17
H_2-Kr[a]	16.0	−2.79	3.26

[a]Ref. [38], the sign of A is unknown.

tion were taken to be of Lennard-Jones (6-12) form [40]. The International Mathematical and Statistical Library computer routines DCADRE (for numerical integration of a function using cautious adaptive Romberg extrapolation) and DMLIN (for numerical integration of a function of several variables with a hyper-rectangle method) were employed in a FORTRAN program for the fitting procedure. For the integral equations, the solution is not unique. It is known that the value of $(BR_0)^{-1}$ for H_2-He is about 0.11 [41,42]. We adopt the same value for HD-Ne and HD-N_2 [38]. The estimated values of A, B, and R_0 for HD-Ne and HD-N_2 together with those estimated for H_2-Ar and H_2-Kr by Poll and Hunt [38] are presented in Table V; the corresponding functions are plotted in Fig. 3. The accuracy of the estimated value depends on the accuracy of the interference parameter a and the potential model, and thus is hard to determine. From the

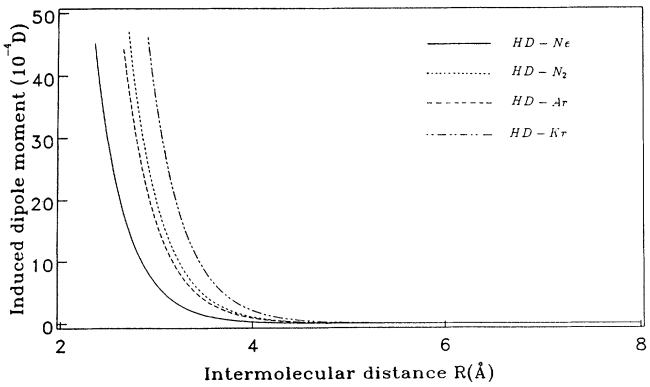

FIG. 3. Estimated magnitude of the induced dipole moment for HD-Ne, HD-N_2, H_2-Ar, and H_2-Kr as a function of intermolecular distance R.

point of view that the induced dipole moment is roughly proportional to the polarizability of the perturber molecule [24], the above estimated values are of the correct order. The possibility of the deduction of such information provides another justification for further experimental and theoretical study of the interference parameter a.

C. Interference parameter $N_0\Delta''I$

The experimental $N_0\Delta''I$ are listed in Table VI. Unlike the vibration-rotational band of HD-HD [43–46], the

TABLE VI. Interference parameter $N_0\Delta''I$ (10^{-4} amagat^{-1}). The uncertainty (1σ) appears in parentheses.

Sample	T (K)	$R(0)$	$R(1)$	$R(2)$	$R(3)$
HD-HD	77[a]	−2.0(8)	−0.7(7)	+1.7(27)	
	195[b]	−0.05(158)	−4.61(76)	−6.01(35)	+12.4(18)
HD-H_2	77[a]	−13(3)	+10(2)	+38(14)	
	195[b]	−4.0(57)	−10.0(10)	−10.1(14)	+10.0(33)
	296[b]		−17.8(50)	+8.6(27)	+8.9(31)
HD-He	77[a]	+15(3)	+13(3)	+40(10)	
	77[c]	+6	−0.3	−13	
	195[a]	+17(12)	+10.9(23)	+8.9(33)	+33.4(96)
	195[c]	+7.5	+6.5	+1.6	
HD-Ne	77[a]	+15(3)	+11(2)	−6(30)	
	195[b]	+25.3(52)	+17.5(10)	+11.3(72)	+2.4(20)
HD-Ar	195[b]	−72.5(61)	+8.0(11)	−20.3(15)	+96(23)
	195[c]	−5.5	+1.1	−6.5	
HD-Kr	195[b]	+26.7(66)	+11.1(81)	+29.9(54)	+11(35)
	296[b]		+12.9(25)	+1.0(29)	+0.2(27)
HD-N_2	195[b]	+8.7(83)	+18.4(27)	−20.4(24)	+4.8(34)
	296[b]		+10.2(17)	−4.3(14)	+14.0(63)

[a]Experiment 1 [10].
[b]Experiment 2. This work.
[c]Calculations from [8,24].

asymmetry of the pure rotational line profile is found to be very small. The difficulties in the base-line correction due to the broad collision-induced background make the determination of such a small asymmetry very difficult. Consequently the results for $N_0\Delta''I$ may be even less reliable than that of a. Comparing the experimental interference parameters carefully, one finds that in quite a few cases, even with the uncertainties, the magnitude of $N_0\Delta''I$ is larger than that of $a/2$. For example, HD-H_2 [$R(2)$] at 195 K, HD-He [$R(2)$] at 77 K, HD-Ne [$R(0)$ and $R(1)$] at 195 K, and HD-Ar [$R(0)$ and $R(3)$] at 195 K, etc. This result also occurred in the experimental results [24] in HD-HD [$R(1)$ and $R(2)$] and HD-Ne [$R(1)$] at 296 K. It also appeared in McKellar's experimental results [5] in HD-HD [$R(1)$, $R(2)$, and $R(3)$]. From the theory of Herman, Tipping, and Poll, the ρ^2 term arises purely from the intercollisional interference or the *scalar* interference, which should be always positive [15,18,47]. Thus the magnitude of $N_0\Delta'I=a/2$ should be always larger than that of $N_0\Delta''I$ if the theory adequately represents the experimental results.

Comparison can be made in a few cases with calculations based on the GTTC theory [22]. For HD-He and HD-Ar, the orders of magnitude are about the same and at 195 K, both signs agree too (Table VI).

VII. LINE-SHAPE PARAMETERS

A. Broadening coefficient

The experimental half width at half maximum (HWHM) broadening coefficients together with theoretical calculations are presented in Table IX. There is a general tendency in the experimental HWHM broadening coefficients. Generally, B_0 decreases with increasing J for all temperatures and systems [except for $R(0)$ at 77 K], and increases with increasing temperature at all J for all systems [except for $R(3)$ at 296 K for several systems]. The reason behind the tendency is the fact that as J increases, the energy gap between the rotational energy level $E(J)$ and $E(J+1)$ increases, thereby reducing the efficiency of inelastic transitions between adjacent levels, giving rise to longer coherence times. On the other hand, generally, when the temperature increases, the relative velocity of the molecules increases, thereby increasing the frequency of collision between absorber and perturber molecules, resulting in the increase of the broadening coefficient. The impact theory suggests a simple power law describing the temperature dependence of the linewidth [48,49]:

$$\gamma_{0H}(T)=\gamma_{0H}(T_{\rm ref})(T/T_{\rm ref})^N , \tag{31}$$

where γ_{0H} is the HWHM, T is the temperature, and $T_{\rm ref}$ is the reference temperature. If this is true, the broadening coefficient should obey the same rule,

$$B_0(T)=B_0(T_{\rm ref})(T/T_{\rm ref})^N . \tag{32}$$

The exponents N deduced from the experimental broadening coefficients are presented in Table VII. In general, the N for all systems are reasonably consistent within their uncertainties at different temperatures for a given $R(J)$ and system. This fact may provide evidence for the validity of the simple power law to describe the temperature dependence of linewidth to some degree. However, only three temperatures are involved and such a generalization may not be appropriate.

TABLE VII. N deduced from experimental broadening coefficients. Uncertainty (1σ) appears in parentheses. $T_{\rm ref}=77$ K.

System	T (K)	N $R(0)$	$R(1)$	$R(2)$
HD-HD	195	1.31(6)	0.65(1)	0.68(4)
	296	1.34(7)	0.78(4)	0.74(1)
HD-H_2	195		0.71(8)	0.96(10)
	296		0.78(2)	0.82(7)
HD-He	195		1.02(5)	1.31(13)
	296		1.26(4)	1.29(9)
HD-Ne	195		0.66(3)	1.12(22)
	296		0.69(3)	1.05(17)

To investigate the overall behavior of the broadening coefficient among different systems, the linewidth was calculated by using a simplified model within a semiclassical theory developed by Bonamy and Robert, described in detail in Refs. [49] and [50]. The intermolecular potential used was an *atomic* site model [35]. This model describes the molecular interaction as the superposition of *atom-atom* interactions in the collision pair [50,51],

$$V=\sum_{i,j}\left[\frac{d_{ij}}{r_{1i,2j}^{12}}-\frac{e_{ij}}{r_{1i,2j}^{6}}\right]+V_{\mu_1\mu_2}+V_{\mu_1 Q_2}+\cdots , \tag{33}$$

where the indices i and j refer to the ith atom of molecule 1 and the jth atom of molecule 2, $r_{1i,2j}$ is the distance between these two atoms, d_{ij} and e_{ij} are the atomic-pair energy parameters, and μ and Q are the permanent dipole and quadrupole moment, respectively, of the colliding molecules. If the imaginary part of the differential cross section is neglected, as is frequently done in line-broadening calculations [49], a simplified form for HWHM results,

$$\gamma_H=\frac{N_b}{2\pi c}\bar{v}\sum_{j_2}\rho_{j_2}\int_0^\infty 2\pi b\,(1-e^{\zeta_2(b,\bar{v})})db , \tag{34}$$

where $\bar{v}$ is the mean velocity from Maxwell distribution and

$$\zeta_2(b,v)=S_{2,f2}+S_{2,i2}+S_{2,f2,i2}^{(c)} . \tag{35}$$

In the numerical calculations, only atom-atom contributions to the intermolecular potential are of importance. The pair energy parameters d_{ij} and e_{ij} and the *Lennard-Jones* parameters for the collision pair were evaluated through the usual combination rules [52,53], $\epsilon_{12}=(\epsilon_1\epsilon_2)^{1/2}$, $\sigma_{12}=(\sigma_1+\sigma_2)/2$, $e_{12}=(e_1e_2)^{1/2}$, and $d_{12}=e_{12}(\sigma_{12})^6$, where e_i was obtained from the atomic *Lennard-Jones* parameters ϵ_i and σ_i by [50] $e_i=\epsilon_i\sigma_i^6$ and

TABLE VIII. Parameters used in the line-broadening calculations.

Sample	σ_{12} (Å)	ϵ_{12}/k (K)	e_{ij} (10^{-12} erg Å^6)	d_{ij} (10^{-8} erg Å^{12})	B_{01} (cm^{-1})	B_{02} (cm^{-1})
HD-HD[a]	2.96	36.4	3.37	0.225	44.66	44.66
HD-H_2	2.96	36.4	3.37	0.225	44.66	44.66
HD-He[b]	2.75	19.27	1.14	0.05	44.66	0.0
HD-Ne[b]	2.87	33.7	2.70	0.15	44.66	0.0
HD-Ar[b]	3.27	66.09	9.64	1.03	44.66	0.0
HD-Kr[b]	3.28	79.0	12.2	1.5	44.66	0.0
HD-N_2[b]	3.30	57.66	10.3	1.38	44.66	2.0

[a]Deduced from LJ potential parameters taken from Ref. [39].
[b]Deduced from LJ potential parameters from the average value of Ref. [40].

$d_i = e_i \sigma_i^6$. The computation program used was the code of Bonamy originally developed for CO-Ar, and modified to suit our cases. The important parameters used in the calculations are listed in Table VIII. As can be seen in Table IX, HWHM broadening coefficients consistently agree with the general tendency of the J dependence and temperature dependence of the experimental results. However, quantitatively, this calculation overestimates B_{0H} at 296 K and for low-J lines. The calculated results agree better for $R(2)$ and $R(3)$, and for the cases where HD is perturbed by large molecules. The source of the discrepancy is probably due to the classical trajectory approximation, which may not be proper for light molecules such as HD. Moreover, the decoupling between translation and rotation for the molecule HD is questionable [54]. In addition, in this simplified model, the higher-order terms of the angular dependent potential, as well as the static electric contributions are neglected, while the linewidth is sensitive to short-range anisotropic interactions [22,51]. Finally, as is well known, the atom-atom potential model is incorrect at long range [55]. This inadequacy will affect the calculation, particularly at low temperatures.

There is an exception to the general tendency of the J dependence in that the broadening coefficients for $R(0)$ at 77 K for HD-HD, HD-H_2, HD-He, and HD-Ne are all clearly lower than those for $R(1)$ for the same systems. This cannot be attributed to the experimental uncertainty

TABLE IX. Calculated and experimental values of HWHM broadening coefficients B_{0H} (10^{-2} cm^{-1} amagat^{-1}).

Sample	T (K)	$R(0)$ Expt.	$R(0)$ Calc.	$R(1)$ Expt.	$R(1)$ Calc.	$R(2)$ Expt.	$R(2)$ Calc.	$R(3)$ Expt.	$R(3)$ Calc.
HD-HD	77	0.27	0.85	0.44	0.58	0.41	0.29		
	195	0.90	2.1	0.81	1.6	0.75	1.2	0.62	0.7
	296	1.7	3.1	1.3	2.5	1.1	1.9	0.90	1.4
HD-H_2	77	0.29	0.82	0.40	0.55	0.31	0.29		
	195	0.90	2.0	0.76	1.6	0.78	1.2	0.65	0.7
	296			1.1	2.5	0.95	1.9	1.0	1.4
HD-He	77	0.15	0.61	0.20	0.41	0.12	0.19		
	195	0.52	1.7	0.51	1.3	0.41	0.91	0.38	0.55
	296			1.1	2.0	0.68	1.6	0.59	1.1
HD-Ne	77	0.24	0.80	0.33	0.51	0.18	0.21		
	195	0.80	1.8	0.61	1.4	0.52	0.88	0.48	0.47
	296			0.84	2.1	0.75	1.5	0.34	0.98
HD-Ar	195	1.4	1.6	1.0	1.1	0.86	0.64	0.63	0.29
	296			1.5	1.8	1.1	1.2	0.68	0.67
HD-Kr	195	1.5	2.1	1.2	1.5	1.1	0.87	0.91	0.39
	296			1.3	2.4	0.99	1.5	0.54	0.84
HD-N_2	195	2.1	2.6	1.4	1.9	0.99	1.1	0.84	0.51
	296			1.4	2.8	1.4	1.9	0.68	1.1

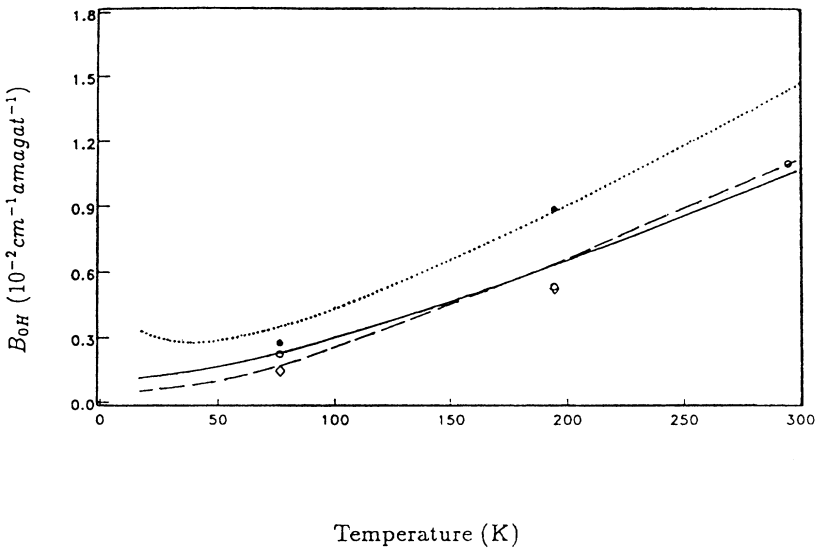

FIG. 4. HWHM broadening coefficient B_{0H} (10^{-2} cm^{-1} amagat^{-1}) for HD-H_2 and HD-He as a function of temperature. ●, $R(0)$, HD-H_2, experimental; ◇, $R(0)$, HD-He, experimental; ○, $R(1)$, HD-He, experimental. Dotted line, $R(0)$, HD-H_2, deduced from Ref. [56]; dashed line, $R(0)$, HD-He, deduced from Ref. [56]; solid line, $R(1)$, HD-He, deduced from Ref. [56].

because of the good quality of the $R(0)$ spectra at 77 K and the large difference between the broadening coefficients for $R(0)$ and $R(1)$. However the observed anomalous behavior is confirmed by a quantum-mechanical calculation by Schaefer and Monchick [56]. They calculated the pressure-broadening line-shape cross section for HD-H_2 and HD-He with the Ben-Reuven-Fano-Baranger formalism. The potential used in their calculation was a six-term Legendre polynomial expansion grid. Their calculation is in excellent agreement with our experimental results. Whether this type of calculation gives consistent results for $R(2)$ and $R(3)$ as well as for other systems remains unknown. The HWHM deduced from their calculated line-shape cross section and the corresponding experimental HWHM broadening coefficient B_{oH} are collected in Table X and plotted in Fig. 4.

TABLE X. Comparison of experimental and theoretical HWHM broadening coefficients B_{0H} (10^{-2} cm^{-1} amagat^{-1}) for $R(0)$ and $R(1)$ for HD-H_2 and HD-He. Uncertainty (1σ) appears in parentheses.

Reference	System	T (K)	B_0 $R(0)$	B_0 $R(1)$
		Experiment		
Present work	HD-H_2	77	0.28(2)	
		195	0.89(2)	
	HD-He	77	0.15(1)	0.20(1)
		195	0.53(6)	0.51(1)
Experiment 3[a]		296		1.07(3)
		Calculation		
Schaefer and Monchick[b]	HD-H_2	77	0.35	
		195	0.89	
	HD-He	77	0.17	0.22
		195	0.64	0.62
		296		1.05

[a]Reference [8,24].
[b]Reference [56].

B. Absolute frequency and frequency-shift coefficient

Now we turn to the absolute frequencies of the four pure rotational lines of HD and the frequency-shift coefficients for HD-HD and HD-X systems. The absolute frequency measured in this laboratory is quite consistent in the experiments [8,10,35]. The average values of the frequency determinations for $R(0)$ to $R(3)$ are, respectively, 89.21(1), 177.84(1), 265.24(1), and 350.86(1), in cm^{-1}. As for the broadening coefficient, the frequency-shift coefficients in Table XI show a general tendency in J dependence and temperature dependence. Specifically, S_0 goes from positive (blue shift) to negative (red shift) for all systems at all temperatures with increasing J, and S_0 increases with increasing temperature at a given J for most cases. A comparison with theoretical calculation of Schaefer and Monchick is shown in Table XII. The values of S_0 for $R(0)$ for HD-H_2, and for $R(0)$ and $R(1)$ for HD-He agree very well for our experimental result and the theoretical calculations. This result suggests that our frequency-shift coefficients are generally accurate.

VIII. FURTHER DISCUSSION AND CONCLUSIONS

Characterization of the density and temperature dependence of the spectral line-shape parameters and absorption coefficients for the pure rotational band of gaseous HD is reasonably complete based on the experiments at 77, 195, and 296 K in this laboratory. The refined values of the allowed dipole-moment matrix elements show a different J dependence from the predictions of the theory, although within the 99% confidence error bar, the J dependence predicted by Wolniewicz is possible. The averaged *ab initio* calculations agree well with (but are about 3% larger than) the experimental determinations. The theoretical calculation of the interference effects for the pure rotational band of HD-HD and HD-X

TABLE XI. Frequency-shift coefficients S_0 (10^{-3} cm^{-1} amagat^{-1}). + and − refer to *blue* and *red* shifts, respectively. The uncertainty (1σ) appears in parentheses.

Sample	T (K)	$R(0)$	$R(1)$	$R(2)$	$R(3)$
HD-HD	77[a]	+0.305(67)	+0.074(18)	−0.24(10)	
	195[b]	+1.07(4)	+1.21(4)	+0.61(4)	−0.31(8)
	296[c]	+3.5(5)	+0.6(1)	+0.6(1)	−0.4(1)
HD-H_2	77[a]	+0.31(5)	+0.37(3)	−3.15(31)	
	195[b]	+1.02(26)	+1.15(5)	+0.64(8)	−2.4(7)
	296[b]		+1.51(25)	+0.29(13)	−3.01(44)
HD-He	77[a]	+0.58(4)	+0.65(3)	−1.11(22)	
	195[a]	+0.98(13)	+2.15(12)	+1.22(8)	−0.45(58)
	296[c]		+2.4(2)	+2.8(1)	+1.8(3)
HD-Ne	77[a]	+1.01(6)	+1.13(5)	−0.86(32)	
	195[b]	+0.98(13)	+1.76(4)	+0.32(4)	+0.87(28)
	296[c]		+4.4(1)	+2.4(1)	+0.3(2)
HD-Ar	195[b]	+4.78(47)	+2.51(7)	+0.51(8)	−5.8(3)
	296[b]		+8.3(3)	+1.3(1)	−1.1(2)
HD-Kr	195[b]	1.6(1)	+3.28(2)	−3.0(17)	−5.4(5)
	296[b]		+3.52(23)	−0.515(54)	−2.03(16)
HD-N_2	195[b]	+2.08(57)	+3.54(10)	+0.17(11)	−3.11(47)
	296[b]		+5.28(16)	+0.713(99)	−2.65(33)

[a]Experiment 1 [10].
[b]Experiment 2. This work.
[c]Experiment 3 [8,24].

are generally consistent with the experimental determinations with respect to order of magnitude, but quantitatively, relatively good agreement is achieved only for $R(2)$ and $R(3)$ for HD-atom systems. This result is not surprising since as J increases the importance of J-changing collisions decreases [22]. There is an obvious J dependence in the interference effects from the experimental results that is not predicted by the theory. Furthermore a change in sign of the interference parameter a with temperature at constant J for HD-HD and HD-X is evident in the experiment but not predicted by the theory. From the theory, the temperature enters the calculation of a through the pair distribution function by which the average dipole moment has a small temperature dependence [16]. The refinements due to rotational-level mixing and near-resonance rotational-level mixing improve the agreement between theory and experiment to some degree but still give results not consistent with experiment both with respect to sign and magnitude. The discrepancies may be due to the phase factor Δ', but the ratio of a/a_{theory} in Table XIII shows that about one-third of the corresponding Δ' including their uncertainties are larger than unity. The method of introduction of Δ into the theory requires, however, that the absolute magnitude of either Δ' or Δ'' never exceed unity [16]. These facts may indicate that the mechanism in the interference effects in the pure rotational band for gaseous HD-HD and for the low-J lines of HD-X, are more complicated than the description in the pioneering theory of Herman, Tipping, and Poll, which applies to the special case where the propagator is diagonal and only pure elastic collisions are permitted [21]. Many of these observed effects are accounted for at least qualitatively by the theory of GTTC [21,22]. We note the

TABLE XII. Comparison of experimental and theoretical frequency-shift coefficients (10^{-3} cm^{-1} amagat^{-1}) for $R(0)$ and $R(1)$ for HD-H_2 and HD-He. Uncertainty (1σ) appears in parentheses.

Reference	System	T (K)	S_0 $R(0)$	S_0 $R(1)$
		Experiment		
Present work	HD-H_2	77	0.31(5)	
		195	1.02(26)	
	HD-He	77	0.58(4)	0.65(31)
		195	0.98(53)	2.15(12)
Experiment 3[a]		296		2.4(2)
		Calculation		
Schaefer and Monchick[b]	HD-H_2	77	0.46	
		195	1.03	
	HD-He	77	0.73	1.03
		195	1.28	2.06
		296		2.50

[a]Reference [8,24].
[b]Reference [56].

TABLE XIII. Ratio of a/a_{theory}. The uncertainty (1σ) appears in parentheses.

System	T (K)	a/a_{theory} $R(0)$	$R(1)$	$R(2)$	$R(3)$
HD-HD	77	+2.3(3)	+2.1(2)	+1.5(3)	
	195	−1.3(1)	−0.3(1)	−0.1(1)	−9.8(5)
	296	−1.2(9)	−0.7(1)	−0.8(1)	+1.6(5)
HD-H_2	77	+5.1(14)	+3.0(19)	+1.1(40)	
	195	+1.1(7)	−2.3(4)	+0.1(3)	−5.3(35)
	296		−4.6(7)	+5.0(5)	−2.9(12)
HD-He	77	+1.3(4)	+1.4(2)	+1.0(3)	
	195	−1.8(6)	−0.1(1)	+0.4(1)	+0.6(5)
	296		+0.8(1)	+0.5(1)	+1.3(3)
HD-Ar	195	+0.1(1)	−0.4(1)	+1.1(7)	+0.3(4)
	296		+0.2(1)	+0.6(1)	+1.0(1)
HD-Kr[a]	195	0.3(1)	1.6(2)	1.0(2)	1.2(8)
	296		1.6(1)	0.7(1)	0.6(1)

[a]The sign of induced moment is unknown.

possibility that the temperature dependence may come through the J dependence of the induced dipole matrix elements [9]. However, whether it explains the sign-change behavior of the temperature-dependent interference effect must await the detailed calculations of the induced dipole matrix elements. The line-broadening coefficients for the pure rotational band, calculated through a simplified model within semiclassical theory, agree with the general trends and order of magnitude of the experimental determinations. Better agreement is found for $R(2)$ and $R(3)$, and for HD perturbed with large atoms. Quantum-mechanical calculations for $R(0)$ and $R(1)$ for HD-H_2 and HD-He [56] are found to be in very good agreement with the experimental results for both the line-broadening coefficient and frequency shift. This fact suggests, as expected, that for the small molecule collision pair such as HD-HD, HD-H_2, HD-He and perhaps HD-Ne, a quantum-mechanical calculation is more suitable.

ACKNOWLEDGMENTS

This research was supported by the Natural Science and Engineering Research Council of Canada. One of the authors (Z.L.) wishes to thank J. Bonamy for her generous help in the linewidth calculations, and the University of Manitoba for support.

*Present address: Herzberg Institute of Astrophysics, National Research Council, Ottawa, Ontario, Canada K1A 0R6.

[1] J. B. Nelson and G. C. Tabisz, Phys. Rev. Lett. **48**, 1393 (1982).
[2] J. B. Nelson and G. C. Tabisz, Phys. Rev. A **28**, 2157 (1983).
[3] G. C. Tabisz and J. B. Nelson, Phys. Rev. A **31**, 1160 (1985).
[4] A. R. W. McKellar, J. W. C. Johns, W. Majewski, and N. H. Rich, Can. J. Phys. **62**, 1673 (1984).
[5] A. R. W. McKellar, Can. J. Phys. **64**, 227 (1986).
[6] P. Essenwanger and H. P. Gush, Can. J. Phys. **62**, 1680 (1984).
[7] P. Drakopoulos and G. C. Tabisz, Phys. Rev. A **36**, 5556 (1987).
[8] P. Drakoloulos and G. C. Tabisz, Phys. Rev. A **36**, 5566 (1987).
[9] Q. Ma, R. H. Tipping, and J. D. Poll, Phys. Rev. A **38**, 6185 (1988).
[10] L. Ulivi, Z. Lu, and G. C. Tabisz, Phys. Rev. A **40**, 642 (1989).
[11] R. H. Tipping and J. D. Poll, Phys. Rev. B **35**, 6699 (1987).
[12] A. R. W. McKellar and M. J. Clouter, Chem. Phys. Lett. **140**, 117 (1987).
[13] S. Y. Lee, S. Lee, J. Gains, R. H. Tipping, and J. D. Poll, Phys. Rev. B **37**, 2357 (1988).
[14] R. H. Tipping, J. D. Poll, and A. R. W. McKellar, Can. J. Phys. **56**, 75 (1978).
[15] R. M. Herman, Phys. Rev. Lett. **42**, 1206 (1979).
[16] R. M. Herman, R. H. Tipping, and J. D. Poll, Phys. Rev. A **20**, 2006 (1979).
[17] R. H. Tipping and J. D. Poll, in *Molecular Spectroscopy: Modern Research*, edited by K. N. Rao (Academic, New York, 1985), Vol. III, p. 421.
[18] J. D. Poll, in *Phenomena Induced by Intermolecular Interactions*, edited by G. Birnbaum (Plenum, New York, 1985), p. 677.
[19] M. E. Rose, *Elementary Theory of Angular Momentum* (Wiley, New York, 1957), p. 222.

[20] J. D. Poll and J. Van Kranendonk, Can. J. Phys. **39**, 189 (1961).
[21] B. Gao, G. C. Tabisz, M. Trippenbach, and J. Cooper, Phys. Rev. A **44**, 7379 (1991).
[22] B. Gao, J. Cooper, and G. C. Tabisz, Phys. Rev. A **46**, 5781 (1992).
[23] J. H. Dymond and E. B. Smith, *The Virial Coefficients of Pure Gases and Mixtures* (Clarendon, Oxford, 1980).
[24] P. Drakopoulos, Ph.D. thesis, University of Manitoba, 1987.
[25] P. W. Atkins, *Physical Chemistry* (Freeman, San Francisco, 1978), p. 771.
[26] A. K. Kudian and H. L. Welsh, Can. J. Phys. **49**, 230 (1971).
[27] User's Manual of Nic-7199 FT-IR System, Nicolet Analytical Instruments (1979).
[28] J. W. C. Johns, J. Opt. Soc. Am. B **2**, 1340 (1985).
[29] A. L. Ford and J. C. Browne, Phys. Rev. A **16**, 1992 (1977).
[30] W. R. Thorson, J. H. Choi, and S. K. Knudson, Phys. Rev. A **31**, 34 (1985).
[31] D. Bishop and L. Cheung, Chem. Phys. Lett. **55**, 593 (1978).
[32] L. Wolniewicz, Can. J. Phys. **54**, 572 (1976).
[33] P. R. Bunker, J. Mol. Spectrosc. **46**, 119 (1973).
[34] M. Trefler and H. P. Gush, Phys. Rev. Lett. **20**, 703 (1968).
[35] Z. Lu, Ph.D. thesis, University of Manitoba, 1991.
[36] J. D. Poll and M. S. Miller, J. Chem. Phys. **54**, 2673 (1971).
[37] A. Borysow, L. Frommhold, and W. Meyer, J. Chem. Phys. **88**, 4855 (1988).
[38] J. D. Poll and J. L. Hunt, Can. J. Phys. **54**, 461 (1976).
[39] J. Bonamy, L. Bonamy, and D. Robert, J. Chem. Phys. **67**, 4441 (1977).
[40] J. O. Hirschfelder, C. F. Curtiss, and R. B. Bird, *Molecular Theory of Gases and Liquids* (Wiley, New York, 1954).
[41] L. Trafton, Astrophys. J. **179**, 971 (1973).
[42] J. D. Poll, J. L. Hunt, and J. W. Mactaggart, Can. J. Phys. **53**, 954 (1975).
[43] A. R. W. McKellar, Astrophys. J. Lett. **185**, L53 (1973).
[44] A. R. W. McKellar, Can. J. Phys. **51**, 389 (1973).
[45] A. R. W. McKellar, J. Chem. Phys. **52**, 1144 (1974).
[46] A. R. W. McKellar, Can. J. Phys. **61**, 4636 (1974).
[47] R. M. Herman, in *Spectral Line Shapes IV*, edited by J. Exton (Deepak, Hampton, 1987), p. 351.
[48] G. Birnbaum, Adv. Chem. Phys. **12**, 4870 (1967).
[49] J. Bonamy and D. Robert, J. Quant. Spectrosc. Radiat. Transfer **31**, 23 (1984).
[50] D. Robert and J. Bonamy, J. Phys. **40**, 923 (1979).
[51] N. Lacome and A. Levy, J. Mol. Spectrosc. **97**, 139 (1983).
[52] J. P. Looney, Ph.D thesis, Pennsylvania State University, 1987.
[53] M. Oobatake and T. Ooi, Prog. Theor. Phys. **48**, 2132 (1972).
[54] J. Bonamy (private communication).
[55] C. G. Gray and K. E. Gubbins, *Theory of Molecular Fluids* (Oxford, New York, 1984).
[56] J. Schaefer and L. Monchick, J. Chem. Phys. **87**, 171 (1987).